RMetS
Royal Meteorological Society

ENSO influence upon global temperature in nature and in CMIP5 simulations

Victor Privalsky[1]* and Vladislav Yushkov[2]

[1]*N.N. Zubov State Oceanographic Institute, Moscow, Russia*
[2]*Physics Department, Moscow State University, Russia*

*Correspondence to:
V. Privalsky, N.N. Zubov State
Oceanographic Institute,
Moscow, Russia.
E-mail:
vprivalsky@oceanography.ru*

Abstract

Statistical properties of observed and CMIP5-simulated bivariate time series 'annual global surface temperature (AGST) – sea surface temperature in the Niño area 3.4 (SST3.4)' are analyzed in the time and frequency domains. Both observed and most simulated data show that AGST is explicitly affected by SST3.4 but not vice versa. Though the AGST spectral density is low at intermediate frequencies, most CMIP5 models reproduce its behavior and show the high coherence observed in nature inside that frequency band. However, CMIP5 models show a dependence between AGST and SST3.4 at frequencies below $0.1\,\text{year}^{-1}$, which is not found in nature.

Keywords: global temperature and ENSO; teleconnections; bivariate time series analysis; time and frequency domains; validation of CMIP5 models

1. Introduction

The El Niño-Southern Oscillation (ENSO) system presents a unique example of interannual variability within the Earth's climate system and is believed to affect the global surface temperature (e.g. Jones, 1988; Privalsky and Jensen, 1995). As high coherence between global and regional processes is a rare occurrence in the Earth's climate, such phenomena present a convenient tool for validation of climate models.

The important role of ENSO in climate modeling has been recognized earlier, and climate models were validated with regard to their ability to reproduce ENSO's behavior and its effects upon different elements of climate over the globe. Thus, Bellenger *et al.* (2014) studied many ENSO features, including its amplitudes, seasonality, spectra, etc., and found 'no quantum leap' in the quality of 24 CMIP5 models as compared to the previous CMIP3 versions. A mostly frequency domain validation of CMIP5 models was presented in Privalsky and Yushkov (2014) who found that the uniquely strong teleconnection within ENSO between the annual sea surface temperature in the El Niño area 3.4 and the annual sea level pressure differences Tahiti–Darwin (SOI) is properly reproduced by 44 out of the 46 models within the CMIP5 historical experiment.

Several studies used ENSO as a litmus test for the ability of CMIP5 models to reproduce ENSO's influence upon precipitation over the Americas and over Africa (Langenbrunner and Neelin, 2013), Indian Basin Ocean Mode (Tao *et al.*, 2014), and upon early summer climate of North Pacific and East Asia (Hu *et al.*, 2014). These studies do not use spatial averaging and are based, to a large degree, upon thousands of correlation and regression coefficient estimates. Their results concerning the quality of CMIP5 models are rather indefinite.

The approach used in the current study is based upon spatial averaging of observation data – global for AGST and regional for SST3.4. This operation allows one to avoid comparisons of sequences of multidimensional random fields by reducing them to time series that depend on just one argument – time (see Privalsky and Croley, 1992). Comparing time series with each other is, of course, much simpler than comparing time-dependent sequences of random fields. By changing the scale of spatial averaging, one can validate climate models presented with sets of time series obtained by spatial averaging, thus getting quantitative statistical information about the models' capabilities at different spatial scales.

Another advantage of the time series approach is the ability to predict natural variations of climate on the basis of the Kolmogorov-Wiener theory of extrapolation; such results can be used to improve climate projections due to the known external forcing by taking into account the probable future behavior of natural climate variations.

In this article, we will study connections between

- the observed annual global surface temperature (AGST) and the oceanic component of the ENSO system – the sea surface temperature in the Niño area 3.4 (SST3.4),
- time series of AGST and SST3.4 generated within the framework of the CMIP5 historical experiment.

The results obtained for the observed time series are compared with respective results for the simulated data in order to determine to what extent the CMIP5 models can reproduce time and frequency domain

features of the observed teleconnection between the global temperature and the ENSO oceanic component. Specifically, we are interested in the contribution of SST3.4 to the annual global surface temperature as seen from respective stochastic difference equations, spectra, coherence functions, and coherent spectra both in nature and in CMIP5 simulations.

2. Data and method

2.1. Data

The time series used here to study connections that exist in the actual climate system contains two components: AGST and SST3.4 from 1876 through 2005 (time series length $N = 130$). Both data sets were obtained from the file HadCRUT4 published at the University of East Anglia web site (Morice *et al.*, 2012).

The ENSO system contains two components: sea surface temperature in western equatorial Pacific and Southern Oscillation index (SOI), which are closely correlated with each other: the cross correlation coefficient -0.83 and the coherence function over 0.9 (Privalsky and Muzylev, 2013). This means that they contain much information about each other and therefore we selected only one time series, namely, the annual values of SST3.4, to analyze observations and compare results of analysis with simulation results. The initial year for the time series was selected having in mind that the Australian sea level pressure data for the second ENSO component – Southern Oscillation Index – is available from 1876. Besides, the SST3.4 data contain over 50% of missing observations within the time interval from 1850 through 1875. The observed time series are shown in Figure 1, and the list of CMIP5 models used in this study is given in Table 1.

The simulated data are taken from the ESGF portal (see Taylor *et al.*, 2012) and include time series of AGST and SST3.4 obtained under the CMIP5 historical experiment for the models listed in Table 1 (one run per model, mostly run 1). All simulation data were masked in accordance with respective observations. The linear trend was always removed from all time series prior to further analysis.

2.2. Method

The method of time series analysis used in this study is based upon the parametric (autoregressive) modeling of multivariate time series in the time and frequency domains. Let $x_{1,n}$ and $x_{2,n}$ be the time series of AGST and SST3.4, respectively. The time series $\mathbf{x}_n = [x_{1,n}, x_{2,n}]'$, $n = 1, 2, \ldots, N$, where $N = 130$ and the strike means matrix transposition, is regarded as a sample of a bivariate linearly regular (specifically, autoregressive) random process, that is,

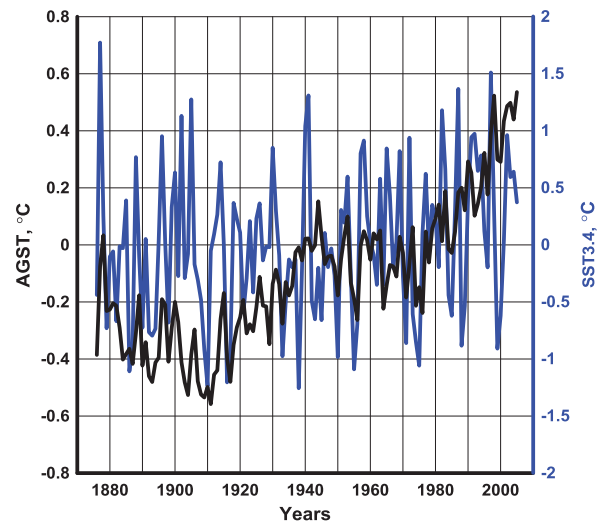$$\mathbf{x}_n = \sum_{j=1}^{p} \mathbf{\Phi}_j \mathbf{x}_{n-j} + \mathbf{a}_n \qquad (1)$$

Figure 1. Time series of AGST (black) and SST3.4 (blue).

Table 1. CMIP5 models used in this work.

Model	Model	Model
ACCESS1.0 (1)[a]	CSIRO-Mk3.6.0 (1)	INM-CM4 (1)
ACCESS1.3 (3)	CSIRO-Mk3L-1-2 (10)	IPSL-CM5A-LR (6)
BCC-CSM1.1 (3)	EC-EARTH	IPSL-CM5A-MR (3)
BCC-CSM1.1(m) (3)	FGOALS-g2 (10)	IPSL-CM5B-LR (1)
BNU-ESM (1)	FIO-ESM (5)	MIROC5 (3)
CanESM2 (5)	GFDL-CM2.1 (12)	MIROC-ESM (3)
CCSM4 (6)	GFDL-CM3 (1)	MIROC-ESM-CHEM
CESM1(BGC) (1)	GFDL-ESM2G (3)	MPI-ESM-LR (3)
CESM1(CAM5) (3)	GFDL-ESM2M (1)	MPI-ESM-MR (3)
CESM1(FASTCHEM) (4)	GISS-E2-H (1)	MPI-ESM-P (2)
CESM1(WCCM) (3)	GISS-E2-H-CC (17)	MRI-CGCM3 (5)
CMCC-CESM (4)	GISS-E2-R (1)	MRI-ESM1 (1)
CMCC-CM (1)	GISS-E2-R-CC (24)	NorESM1-M (3)
CMCC-CMS (1)	HadCM3 (10)	NorESM1-ME (1)
CNRM-CM5 (1)	HadGEM2-CC (3)	
CNRM-CM5-2 (10)	HadGEM2-ES (5)	

[a]Numbers in parentheses show the number of model runs.

Here p is the order of autoregression,

$$\mathbf{\Phi}_j = \begin{bmatrix} \phi_{11}^{(j)} & \phi_{12}^{(j)} \\ \phi_{21}^{(j)} & \phi_{22}^{(j)} \end{bmatrix} \qquad (2)$$

are matrix autoregressive (AR) coefficients, and $\mathbf{a}_n = [a_{1,n}, a_{2,n}]'$ is a (zero mean) bivariate white noise (the innovation sequence) with a covariance matrix

$$\mathbf{R_a} = \begin{bmatrix} R_{11} & R_{12} \\ R_{21} & R_{22} \end{bmatrix} \qquad (3)$$

The quantities R_{11} and R_{22} are the variances and $R_{12} = R_{21}$ covariances, of the innovation sequence components $a_{1,n}$ and $a_{2,n}$. The autoregressive approach is both feasible and appropriate in time series analysis, especially in situations when the time series is short, as in our case (e.g. Jaynes, 1982).

Estimates of the AR order p, matrix AR coefficients $\mathbf{\Phi}_j$, $j = 1, 2, \ldots, p$, and the white noise covariance matrix $\mathbf{R_a}$ are required in order to describe properties of the time series $\mathbf{x}_n$ in time and frequency domains.

The scalar time series AGST $x_{1,n}$ and SST3.4 $x_{2,n}$ are regarded as the output and input, respectively, of a linear system, which is described in the time domain with the stochastic difference Equation (1). The matrices (2) and (3) are estimated here by using the multivariate version of the Levinson's algorithm while the optimal order p of autoregression is selected on the basis of four criteria: Akaike's AIC, Schwarz-Rissanen's BIC, Parzen's CAT, and Hennan-Quinn's Ψ (e.g. Box *et al.*, 2008).

It can be easily shown that the spectral matrix $\mathbf{s}(f)$ that corresponds to Equation (1) is

$$\mathbf{s}(f) = \frac{2\,|\mathbf{R_a}|\,\Delta t}{\left| \mathbf{I} - \sum_{j=1}^{p} \mathbf{\Phi}_j \exp\left(-i2\pi jf\Delta t\right) \right|^2}, 0 \leq f \leq 1/2\Delta t, \tag{4}$$

where $\mathbf{I}$ is the identity 2×2 matrix, $|\mathbf{R_a}|$ the determinant of the matrix $\mathbf{R_a}$, Δt the unit time step (one year in our case), f the cyclic frequency (year^{-1}), and $i = \sqrt{-1}$.

The elements of the spectral matrix

$$\mathbf{s}(f) = \begin{bmatrix} s_{11}(f) & s_{12}(f) \\ s_{21}(f) & s_{22}(f) \end{bmatrix} \tag{5}$$

are the spectral densities $s_{11}(f)$ and $s_{22}(f)$ of the output $x_{1,n}$ (AGST) and the input $x_{2,n}$ (SST3.4), respectively, while $s_{12}(f) = \bar{s}_{21}(f)$ are the complex-valued cross-spectra (the bar means complex conjugation). These quantities are used to calculate other functions which describe the response of the output component $x_{1,n}$ to the input $x_{2,n}$ in the frequency domain. Here, we will use only the coherence function $Co_{12}(f) = |s_{12}(f)| [s_{11}(f)s_{22}(f)]^{-1/2}$ and the coherent spectrum $Cs_{12}(f) = Co_{12}^2(f)s_{11}(f)$. The former quantity can be regarded as a frequency-dependent sequence of 'correlation coefficients' while the latter one describes the part of the spectrum $s_{11}(f)$ generated due to the linear dependence of $x_{1,n}$ upon $x_{2,n}$.

The approximate confidence intervals for these spectral characteristics can be calculated in accordance with the number of degrees of freedom ν for the spectral estimates (e.g. Bendat and Piersol, 1971); for the autoregressive analysis of bivariate time series, ν can be set equal, as a first approximation, to $N/2p$ (Privalsky *et al.*, 1987).

3. Results and discussion

3.1. Time and frequency domain properties of global surface temperature and sea surface temperature in the Niño area 3.4 in nature

Note first that the use of the linear correlation coefficient as a measure of dependence between time series is generally improper because the spectra of time series components $x_{1,n}$ and $x_{2,n}$ are not necessarily identically shaped and relations between them are frequency-dependent. This has been known since long ago both in theory of random processes (Gelfand and

Yaglom, 1957) and in Earth sciences (e.g. Thompson and Emory, 2004), including, in particular, the influence of ENSO upon the annual global surface temperature (Privalsky and Jensen, 1995).

If one were to use the correlation approach to study relations between the AGST and SST3.4, the results would have been discouraging. The correlation coefficient between the two time series equals 0.35. All one would be able to say is that the connection between the two scalar time series might be statistically significant but definitely very weak. Yet, such conclusion would have been wrong because the proper tool for this purpose in time series analysis is the coherence function. Its estimation within the parametric approach that is used here requires a time domain model of the time series (Equation (1)) and subsequent calculation of the spectral matrix (5). With an autoregressive time domain model, the spectral estimates obtained from AR(p) models (1) with a properly selected order p satisfy the requirements of the maximum entropy method.

The optimal time domain representation for the AGST – SST3.4 system has proven to be an AR model of the form given with Equations (1)–(3) with the order $p = 2$:

$$x_{1,t} \approx 0.55x_{1,t-1} + 0.05x_{2,t-1} + 0.26x_{1,t-2}$$
$$\qquad -0.09x_{1,t-2} + a_{1,t} \tag{6}$$
$$x_{2,t} \approx 0.30x_{2,t-1} - 0.33x_{2,t-2} + a_{2,t}$$

with the innovation covariance matrix

$$\mathbf{R_a} = \begin{bmatrix} 0.0084 & 0.0202 \\ 0.0202 & 0.3350 \end{bmatrix}. \tag{7}$$

This model has been selected by three out of the four order selection criteria used here (all but CAT).

The coefficients $\phi_{21}^{(1)}$ and $\phi_{21}^{(2)}$ are not shown in Equation (6) because their estimates are statistically insignificant. This means that the linear stochastic difference Equation (6) connecting AGST with SST3.4 describes a system without a closed feedback loop: SST3.4 affects AGST but is not affected by it explicitly.

Equation (6) can be used to extrapolate AGST beyond 2005 within the Kolmogorov-Wiener theory to obtain the most probable trajectory of natural climate variations and construct respective confidence bounds. The following three points should be mentioned here:

(a) according to Equation (7), the error variance of extrapolation at a 1 year lead time is 0.0084 °C^2 so that the respective 90% confidence interval is $\pm 1.64\sqrt{0.0084} \approx \pm 0.15$ °C^2;

(b) in our case, the lead time at which the error variance becomes close to the AGST variance (the limit of statistical predictability of AGST) is 5–6 years;

(c) as the variance of AGST (after the linear trend is removed) is 0.021 °C^2, the 90% confidence bound at lead times more than 5–6 years is $\pm 1.64\sqrt{0.021} \approx \pm 0.24$ °C^2.

In other words, the contribution of internal variability of climate to its model-based projections is quite
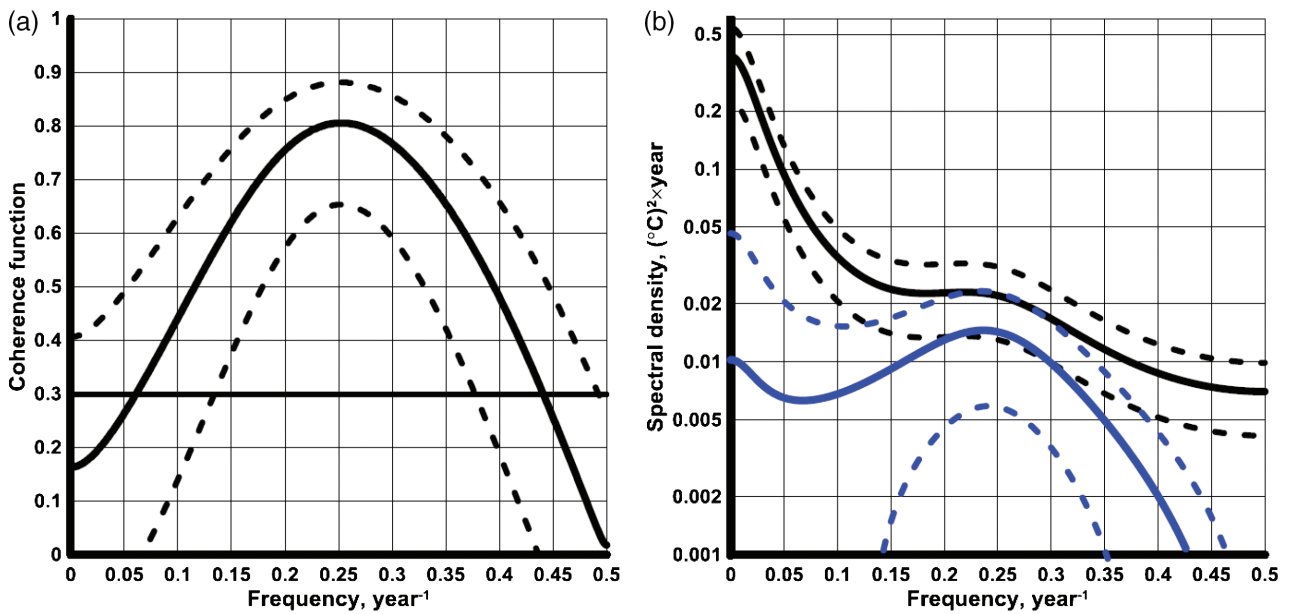
Figure 2. (a) Maximum entropy estimate of coherence between AGST and SST3.4 with approximate 90% confidence bounds (dashed lines); the horizontal line shows the approximate upper 90% confidence limit for the true zero coherence. (b) Maximum entropy estimates of the AGST spectrum (black), and the AGST-SST3.4 coherent spectrum (blue) with approximate 90% confidence limits (dashed lines).
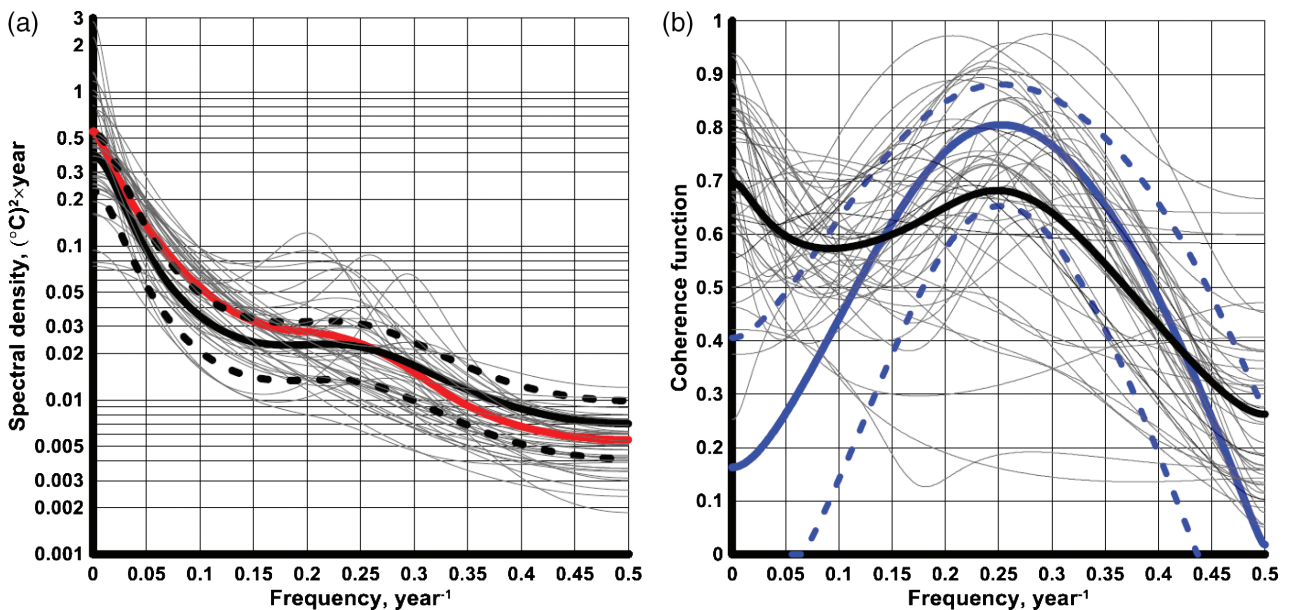
Figure 3. (a) Maximum entropy estimates of the AGST spectrum: observed, with 90% confidence limits (black), simulated (thin lines), and average simulated (red). (b) Maximum entropy estimates of coherence function between AGST and SST3.4 in nature (blue lines, with approximate 90% confidence limits) and in CMIP5 models (thin black lines).

significant (this results disagrees with Yip *et al.*, 2011). A detailed analysis of statistical predictability of the internal variability of climate lies beyond the scope of this short communication.

As seen from Figure 2(a), the coherence function estimate between AGST and SST3.4 grows from practically zero at low frequencies to a maximum of 0.80 at about 0.25 year^{-1} and then decreases to almost zero at higher frequencies. In other words, the annual global surface temperature is closely connected to the sea surface temperature SST3.4 in the Niño area 3.4

but the connection is statistically significant only at intermediate frequencies. Note that the frequency of about 0.24 year^{-1} was found to be the eigen frequency of the damped harmonic oscillator existing, according to analysis of observations from 1876 through 2011, within the ENSO bivariate system (Privalsky and Muzylev, 2013). According to Figure 2(a), the coherence estimate is statistically significant between 0.13 year^{-1} and 0.37 year^{-1}. The linear contribution of SST3.4 to the spectrum of the global surface temperature determined by the square of the coherence

function amounts to 50–60% within the frequency band from 0.18 year^{-1} to 0.33 year^{-1}.

The absolute contribution of SST3.4 to the AGST spectrum shown in Figure 2(b) is statistically significant only within the frequency band from 0.15 year^{-1} to 0.35 year^{-1}, that is, within the band where the coherence function is high but the spectral density of AGST is much lower than at frequencies below 0.1 year^{-1}. This explains why the correlation coefficient between AGST and SST3.4 that 'integrates' the coherence function over the entire frequency band from 0 to 0.5 year^{-1} is low while the coherence function is high. Estimates of the coherent spectrum at low frequencies are statistically insignificant.

3.2. Time and frequency domain properties of global surface temperature and sea surface temperature in the Niño area 3.4 in CMIP5 models

The second goal of this study is to establish whether the CMIP5 models are capable of reproducing the AGST spectrum and the relationship between the annual global surface temperature and ENSO that exists in the actual climate.

Note first that the optimal AR order of simulated bivariate time series was the same as for the observed data ($p = 2$) in 32 cases, with 11 and 3 cases with $p = 1$ and $p = 3$, respectively. The results of time domain analysis were also satisfactory. Though the values of AR coefficients for individual simulated data may differ from respective results for the observed time series, the major time domain conclusion still stands: the sea surface temperature affects the global temperature but is not explicitly affected by it (29 cases against 17).

Within the frequency domain, the estimates of the AGST spectrum obtained from simulated data (Figure 3(a)) show some sample variability but on the whole they reproduce the spectrum of the observed AGST time series quite correctly. The maximum entropy estimates of coherence between simulated time series of AGST and SST3.4 are shown in Figure 3(b). Obviously, most models are capable of reproducing the behavior of the coherence function that exists in nature at the intermediate frequency band. (Unsatisfactory estimates of coherence are given by 11 models.)

The average coherence in simulated data is close to 0.68 at 0.25 year^{-1}. This is an achievement: though the close connection occurs at frequencies where the spectral density of AGST is low, most models discover it.

At the same time, the simulated data reveal a disagreement with nature: most coherence estimates stay statistically significant and keep growing at frequencies below 0.10 year^{-1}; the resulting average 'simulated' coherence (thick black line) differs quite considerably from zero at lower frequencies where the 'observed' coherence is small.

According to Figure 4, the simulated SST3.4 variations more or less correctly describe the role of SST3.4 at frequencies above 0.1 year^{-1} but at lower frequencies simulated data is responsible for 30–50% of the
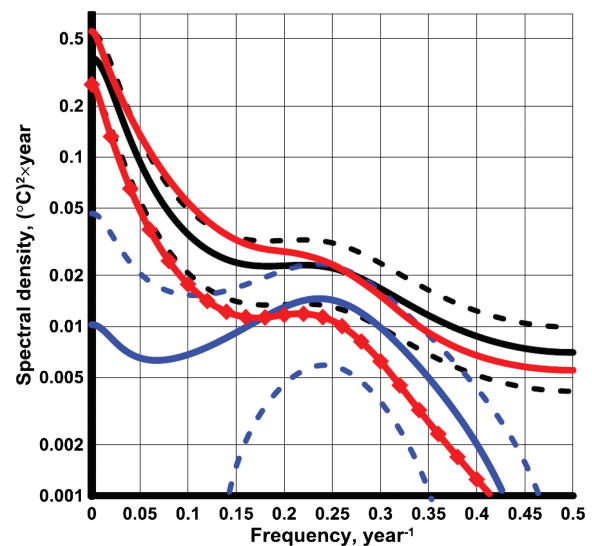
Figure 4. Maximum entropy estimates of SST3.4 spectrum (black lines) and coherent spectrum $Cs_{12}(f)$ AGST-SST3.4 in nature (blue lines), with approximate 90% confidence limits, and the average spectrum and coherent spectrum AGST-SST3.4 in CMIP5 models (red line and red line with symbols).

global temperature spectrum. As the spectral density of AGST at low frequencies is high, this disagreement with observation data means that SST3.4's contribution to the AGST spectrum is higher than it follows from analysis of observations. In other words, the models fail to describe the low-frequency relation between SST3.4 and the global surface temperature that exists in nature.

4. Conclusions

1. The observed bivariate time series 'global surface temperature (AGST) – ENSO's oceanic component (sea surface temperature SST3.4)' presents a linear system with no feedback loop: SST3.4 affects AGST but not vice versa. The simulated time series have the same property in 29 out of the 46 cases. (Note, however, that SST3.4 is affected by AGST indirectly, through the innovation sequence.)

2. The behavior of the annual global surface temperature within the frequency band from about 0.13 year^{-1} to 0.37 year^{-1} is strongly affected by the behavior of ENSO's oceanic component in the same band, with 50–60% of the spectral energy of AGST variations at 0.18–0.33 year^{-1} determined by linear contribution from SST3.4. However, the overall effect of ENSO upon the global temperature is relatively minor because the spectral density of the global surface temperature at those frequencies is small.

3. Time series of AGST generated with CMIP5 models have spectra that usually do not differ significantly from the spectrum of the observed AGST.

4. Most CMIP5 models (35 of the 46) reproduce the general behavior of the coherence function between the observed time series of annual surface

temperature and the oceanic component of ENSO at frequencies higher than 0.15 year^{-1}.

5. At lower frequencies, most estimates of the coherence function between simulated time series grow as frequency diminishes; this disagrees with the behavior of the coherence function estimated on the basis of observation data.

6. According to the simulations, the sea surface temperature in the Niño area 3.4 contributes more energy to the annual global surface temperature at low frequencies than is observed in nature. The relative values of this spurious contribution amount to 30–50% of the AGST's spectral density at frequencies below 0.1 year^{-1}.

On the whole, the ability of most CMIP5 models to detect such a unique and delicate phenomenon in the Earth's climate as a no-feedback-loop connection between the annual global surface temperature and the oceanic component of the El Niño-Southern Oscillation system at intermediate frequencies should be regarded as an achievement. However, the dependence between simulated global temperature and sea surface temperature in the Niño area 3.4 at low frequencies is not found in nature.

References

Bellenger H, Guilyardi E, Leloup J, Lengaigne M, Vialard J. 2014. ENSO representation in climate models: from CMIP3 to CMIP5. *Climate Dynamics* **42**: 1999–2018.

Bendat JS, Piersol AG. 1971. *Random Data. Analysis and Measurements Procedures*, Wiley-Interscience: New York, NY.

Box G, Jenkins G, Reinsel G. 2008. *Time Series Analysis. Forecasting and Control*, 4th ed. John Wiley and Sons: Hoboken, NJ.

Gelfand IM, Yaglom AM. 1957. Calculation of the amount of information about a random function contained in another such function. *Usp. Mat. Nauk*, **12**: 3–52. English translation: *American Mathematical Society. Translation Series 2*, 1959, **12**: 199–246.

Hu K, Huang G, Zheng X-T, Xie S-P, Que Z, Du Y. 2014. Interdecadal variations in ENSO influences on Northwest Pacific–East Asian early summertime climate simulated in CMIP5 Models. *Journal of Climate* **27**: 5982–5998.

Jaynes ET. 1982. On the rational of the maximum-entropy methods. *Proceedings of IEEE* **70**: 939–952.

Jones PD. 1988. The influence of ENSO on global temperatures. *Climate Monitor* **17**: 81–89.

Langenbrunner B, Neelin J. 2013. Analyzing ENSO teleconnections in CMIP models as a measure of model fidelity in simulating precipitation. *Journal of Climate* **26**: 4431–4445.

Morice CP, Kennedy JJ, Rayner NA, Jones PD. 2012. Quantifying uncertainties in global and regional temperature change using an ensemble of observational estimates: the HadCRUT4 dataset. *Journal of Geophysical Research* **117**: D08101, doi: 10.1029/2011JD01 7187.

Privalsky V, Protsenko I, Fogel G. 1987. The sampling variability of autoregressive spectral estimates for two-variate hydrometeorological processes. In Proc. 1st World Congress of the Bernoulli Society for Mathematical Stat., Theory and Applications, Tashkent, USSR, 1986. VNU Science Press, Utrecht, the Netherlands, **2**: 651–654.

Privalsky V, Croley T. 1992. Statistical validation of GCM-simulated climates for U.S. Great Lakes and the C.I.S. Emba and Ural River basins. *Stochastic Hydrology and Hydraulics* **6**: 69–80.

Privalsky VE, Jensen DT. 1995. Assessment of the influence of ENSO on annual global air temperatures. *Dynamics of Atmospheres and Oceans* **22**: 161–178.

Privalsky V, Muzylev S. 2013. An experimental stochastic model of the El Niño-Southern Oscillation system at climatic time scales. *Universal Journal of Geoscience* **1**: 28–36.

Privalsky V, Yushkov V. 2014. Validation of numerical climate models for the El Niño-Southern Oscillation System. *The International Journal of Ocean and Climate Systems* **5**: 1–12.

Tao W, Huang G, Hu K, Qu X, Wen G, Gong H. 2014. Interdecadal modulation of ENSO teleconnections to the Indian Ocean Basin Mode and their relationship under global warming in CMIP5 models. *International Journal of Climatology*, doi: 10.1002/joc.3987.

Taylor KE, Stouffer RJ, Meehl GA. 2012. An overview of CMIP5 and the experiment design. *Bulletin of the American Meteorological Society* **93**: 485–498.

Thompson RE, Emory WJ. 2004. *Data Analysis Methods in Physical Oceanography*, 2nd ed. Elsevier: Amsterdam.

Yip S, Ferro C, Stephenson D. 2011. A simple, coherent framework for partitioning uncertainty in climate predictions. *Journal of Climate* **24**: 4634–4643.